Regional-scale soil salinity assessment using Landsat ETM + canopy reflectance

Elia Scudiero *, Todd H. Skaggs, Dennis L. Corwin

USDA-ARS, United States Salinity Laboratory, 450 West Big Springs Rd., Riverside, CA 92507-4617, USA

ABSTRACT

Soil salinization is widely recognized to be a major threat to worldwide agriculture. Despite decades of research in soil mapping, no reliable and up-to-date salinity maps are available for large geographical regions, especially for the salinity ranges that are most relevant to agricultural productivity (i.e., salinities less than 20 dS m^{-1}, when measured as the electrical conductivity of the soil saturation extract). This paper explores the potentials and limitations of assessing and mapping soil salinity via linear modeling of remote sensing vegetation indices. A case study is presented for western San Joaquin Valley, California, USA using multi-year Landsat 7 ETM + canopy reflectance and the Canopy Response Salinity Index (CRSI). Highly detailed salinity maps for 22 fields comprising 542 ha were used for ground-truthing. Re-gridded to 30 × 30 m, the ground-truth data totaled over 5000 pixels with salinity values in the range 0 to 35.2 dS m^{-1}. Multi-year maximum values of CRSI were used to model soil salinity. Soil type, meteorological data, and crop type were evaluated as covariates. All considered models were evaluated for their fit to the whole data set as well as their performance in a leave-one-field-out spatial cross-validation. The best performing model was a function of CRSI, crop type (i.e., cropped or fallow), rainfall, and average minimum temperature, with $R^2 = 0.728$ when evaluated against all data and $R^2 = 0.611$ for the cross-validation predictions. Broken out by salinity classes, the mean absolute errors (MAE) for the cross-validation predictions were (all units dS m^{-1}): 2.94 for the 0–2 interval (non-saline), 2.12 for 2–4 (slightly saline), 2.35 for 4–8 (moderately saline), 3.23 for 8–16 (strongly saline), and 5.64 for >16 (extremely saline). On a per-field basis, the validation predictions had good agreement with the field average ($R^2 = 0.79$, MAE = 2.46 dS m^{-1}), minimum ($R^2 = 0.76$, MAE = 2.25 dS m^{-1}), and maximum ($R^2 = 0.76$, MAE = 3.09 dS m^{-1}) observed salinity. Overall, reasonably accurate and precise high resolution, regional-scale remote sensing of soil salinity is possible, even over the critical range of 0 to 20 dS m^{-1}, where researchers and policy makers must focus to prevent loss of agricultural productivity and ecosystem health.

Published by Elsevier Inc.

1. Introduction

The degradation of agricultural soil quality due to natural and anthropologic factors is a major concern because it threatens the sustainability and reliability of food production systems (Lobell, 2010). In particular, there is general agreement that soil salinity is a major threat to irrigated and rain-fed agriculture throughout the world (Ghassemi, Jakeman, & Nix, 1995; Ivits, Cherlet, Tóth, Lewińska, & Tóth, 2011). Of the cultivated lands worldwide, about 0.34×10^9 ha (23%) are estimated to be saline, and another 0.56×10^9 ha (37%) are estimated to be sodic (Tanji & Wallender, 2012). To better manage the threat posed by soil salinity, producers, land and water resource managers, and policy makers need reliable, up-to-date, high resolution assessments of soil salinity across large regions. Currently available data are, at best, educated guesses; no reliable inventories based on quantitative ground-truth measurements of soil salinity exist due to the dynamic and complex spatial and temporal nature of salinity (Metternicht & Zinck, 2003). Available regional-scale maps are often qualitative or unreliable (Lal, Iivari, & Kimble, 2004; Lobell et al., 2010).

For years, scientists attempted to use remote sensing to assess soil salinity (Metternicht & Zinck, 2003), although success was limited, especially over very large geographical regions (Lobell et al., 2010). Recently, however, a number of regional-scale studies have indicated a renewed interest in remote sensing approaches (Lobell et al., 2010; Zhang et al., 2011, 2015; Wu, Al-Shafie, Mhaimeed, Ziadat, Nangia, et al., 2014; Wu, Mhaimeed, et al., 2014; Nawar, Buddenbaum, & Hill, 2015; Furby, Caccetta, & Wallace, 2010; Taghizadeh-Mehrjardi, Minasny, Sarmadian, & Malone, 2014; Aldabaa, Weindorf, Chakraborty, Sharma, & Li, 2015; Allbed, Kumar, & Sinha, 2014; Yang, Huang, Liu, Liu, & Zhu, 2015). Unfortunately, most of these studies examined landscapes with salinities far in excess of the range where nearly all agriculture occurs (most halophytes have little commercial value, although there is growing interest in their use as bio-fuel sources; Brown, Cybulska, Chaturvedi, & Thomsen, 2014). The U.S. Salinity Laboratory (U.S. Salinity Laboratory Staff, 1954) classifies agricultural soil salinities as:

0–2 dS m^{-1} (non-saline), 2–4 dS m^{-1} (slightly saline), 4–8 dS m^{-1} (moderately saline), 8–16 dS m^{-1} (strongly saline), and >16 dS m^{-1} (extremely saline), where salinity is quantified as the electrical conductivity of a saturated soil paste extract (EC$_e$, with units of dS m^{-1}). Most of the recent work noted above focused on ranges of 0–100 dS m^{-1} or higher, with little consideration of the reliability or precision of results in the agronomically important range of 0 to 20 or 30 dS m^{-1}.

At EC$_e$ < 20 dS m^{-1}, the ability to directly assess soil salinity from bare soil reflectance is limited (Metternicht & Zinck, 2003; Allbed & Kumar, 2013). In irrigated agriculture, salts do not collect on the surface very often, accumulating instead in the lower portion of the root-zone and below (Skaggs, Anderson, Corwin, & Suarez, 2014). When salinity does exist at the surface, it can be successfully detected with remote sensing techniques, but only in very saline soils, where the influence of vegetation is minimal (Mougenot, Pouget, & Epema, 1993). In lower salinity ranges (0–20 dS m^{-1}), vegetation condition provides a potential alternative proxy of root zone salinity. Generally, when plants experience biotic and abiotic stress (including salinity), their photosynthetic activity decreases, causing increased visible reflectance and reduced near-infrared reflectance (NIR) from the vegetation (Mulla, 2013). Multi-year canopy reflectance data can be used to discriminate landscape features/stressors such as soil salinity that are relatively stable in time (Lobell et al., 2010; Wu, Al-Shafie, et al., 2014; Scudiero, Skaggs, & Corwin, 2014; Lobell, Ortiz-Monasterio, Gurrola, & Valenzuela, 2007) from other stressors that are typically more transient (e.g., drought, pests, and mismanagement) (Scudiero, Teatini, Corwin, Ferro, Simonetti, & Morari, 2014). The pioneering paper of Lobell et al. (2010) used 6 years of MODIS (National Aeronautics and Space Administration Agency, USA) reflectance data (250 × 250 m spatial resolution) to map salinity in the 0–20 dS m^{-1} range in the Red River Valley, USA. More recently, Zhang et al. (2015) used the same satellite sensor to map salinity in the 0–30 dS m^{-1} range for the Yellow River Delta, China. Unfortunately, the resolution of MODIS imagery is generally insufficient to map the spatial variability of salinity that usually exists within agricultural landscapes (Scudiero, Skaggs, & Corwin, 2014; Eldeiry & Garcia, 2008). The 30 × 30 m resolution of the Landsat 7 (L7) Enhanced Thematic Mapper Plus (ETM+) sensor (National Aeronautics and Space Administration Agency and US Geological Survey, USA) offers the possibility of mapping large areas (i.e., at regional scale) with enough detail to allow sub-field management of agricultural farmland. In this context, Landsat 7 represents a viable compromise between spatial resolution and data costs.

Previous studies have shown the importance of including soil-environmental covariates in the salinity assessment models. Soil type, geographical location, meteorological setting (Scudiero, Skaggs, & Corwin, 2014), and crop cover type (Lobell et al., 2010; Zhang et al., 2015) can all be significant covariates. However, the contribution of individual covariates can be inconsistent (Samuel-Rosa, Heuvelink, Vasques, & Anjos, 2015), depending, for example, on the quality of available data and its spatial resolution (Miller, Koszinski, Wehrhan, & Sommer, 2015).

The objective of this study is to map salinity over a large agricultural region in California's Central Valley, USA using multi-year Landsat 7 ETM+ canopy reflectance. In particular, the manuscript focuses on integration of soil-environmental covariates (e.g., soil texture, meteorological conditions, and crop cover type) and validation of the model. The extent of ground-truth data clearly separates this study from previous studies.

2. California's Western San Joaquin Valley

In less than 1% of USA's farmland, the Central Valley of California, which includes the San Joaquin Valley (SJV), the Sacramento Valley, and the Sacramento-San Joaquin Delta, provides about 25% of the USA's table food (Cone, 1997). However, agricultural practices are challenged by extensive areas of salinity and sodicity, particularly in the western San Joaquin Valley (WSJV, Fig. 1). The WSJV soils are derived from saline alluvium originating from California's Southern Coast Range (Scudiero, Skaggs, & Corwin, 2014; Letey & Dinar, 1986). In the early 1980s, Backlund and Hoppes (1984) estimated about 60% (i.e., 9×10^5 ha) of the soils in the WSJV to be saline and/or sodic.

In arid or semi-arid irrigated agricultural areas such as the SJV, sustaining crop production requires irrigation management practices that prevent excessive root zone salt accumulation. Recent studies have shown that some irrigation practices can help reclaim saline-sodic soil, even when saline irrigation water is used (Corwin, Lesch, Oster, & Kaffka, 2006; Corwin, Lesch, Oster, & Kaffka, 2008). The current 4-year drought in California has resulted in irrigation water allocations to farmers being reduced drastically and substantial land in the SJV being left fallow. Drought and salinization often go hand-in-hand. Fallow land, particularly in the WSJV where water tables can be high, can become saline in a relatively short time due to the upward movement of salts in the soil solution (Corwin, 2014). According to the CropScape database (Han, Yang, Di, & Mueller, 2012), during the current California drought that began in 2010, fallow land went from 12.7% (2007–2010 average) to 19.2, 21.0, and 21.6% in 2011, 2012, and 2013, respectively. In 2014, approximately 1.95×10^5 ha of land in the Central Valley was fallow, resulting in $810 million in lost crop revenue (Howitt, Medellín-Azuara, MacEwan, Lund, & Sumner, 2014).

3. Data and methods

3.1. Landsat 7 canopy reflectance

This study considers seven years (2007–2013) of ETM+ canopy reflectance, over five L7 tiles (Fig. 1), covering the entire WSJV, as described by Scudiero, Skaggs, and Corwin (2014). The ETM+ surface reflectance is provided at the resolution of 30 × 30 m in six multispectral bands, namely: blue (B, 450–520 nm), green (G, 520–600 nm), red (R, 630–690 nm), near-infrared (NIR, 770–900 nm), shortwave infrared 1 (IR1, 1550–1750 nm), and shortwave infrared 2 (IR2, 2090–2350 nm). A total number of 366 scenes with cloud coverage <10% were considered. All scenes with cloud coverage <10% were corrected through the Landsat Ecosystem Disturbance Adaptive Processing System (LEDAPS) according to Masek et al. (2006). The missing data due to the failure of the Scan Line Corrector were masked according to Roy et al. (2010). On a yearly basis, the L7 scenes were stacked (average) obtaining seven datasets for each of the six multispectral bands. Yearly values of the Canopy Response Salinity Index (CRSI, unitless) were calculated according to Scudiero, Skaggs, and Corwin (2014):

$$CRSI = \sqrt{\frac{(NIR \times R) - (G \times B)}{(NIR \times R) + (G \times B)}}. \tag{1}$$

From the yearly average CRSI, the multi-year maximum CRSI was calculated at each pixel, similarly to that proposed by Wu, Al-Shafie, et al. (2014). The multi-year maxima approach helps isolate the effects of soil salinity from other, less-stable factors. Indeed Scudiero, Skaggs, and Corwin (2014) found that the relationship between multi-year maxima CRSI and salinity had a correlation coefficient of r = −0.751, whereas the best single year analysis obtained r = −0.630.

Of the many vegetation indices (VIs) usually calculated employing L7 data, the CRSI showed the best fit with soil salinity data in the WSJV (Scudiero, Skaggs, & Corwin, 2014). Moreover, compared to other, more popular VIs such as the Normalized Difference Vegetation Index, NDVI (Rouse, Haas, Schell, & Deering, 1973) and the Enhanced Vegetation Index, EVI (Huete et al., 2002), CRSI showed stronger correlations and higher sensitivity (calculated according to Ji & Peters, 2007) to salinity changes with EC$_e$ > 1 dS m^{-1}. Moreover, although this manuscript considers CRSI for the salinity assessment models, similar results, and equivalent conclusions, can be achieved with NDVI and EVI.
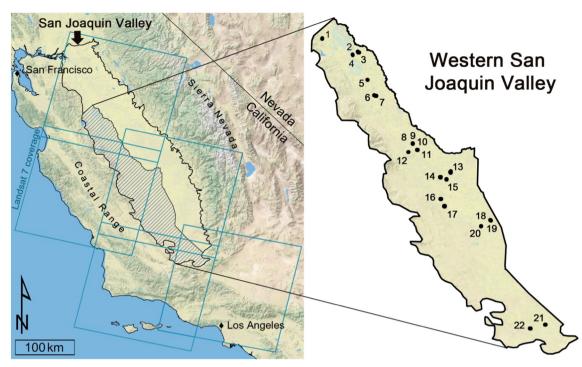
Fig. 1. Map of California's San Joaquin Valley. The western San Joaquin Valley (WSJV) is highlighted with hatch marks. The squares represent the five Landsat 7 tiles covering the WSJV. The location of the 22 study sites is shown in the detailed WSJV map (right). Taken from Scudiero, Skaggs, and Corwin (2014).

3.2. Ground-truth salinity dataset

This study uses the WSJV (Fig. 1) salinity ground-truth measurements presented by Scudiero, Skaggs, and Corwin (2014), to which the reader is referred for detailed description. In 2013, intensive electromagnetic inductions surveys were conducted at 22 agricultural fields (total area 542 ha) collecting 41,779 apparent electrical conductivity (EC$_a$) readings (150 to 13,400 measurements per field, at an average density of ca 175 per ha^{-1}), for both the 0–0.75 and 0–1.50 m soil profiles using an EM38 Dual Dipole (Geonics Ltd., Mississauga, Ontario, Canada) sensor, connected to a GPS and mounted on a non-metallic sled (Corwin & Lesch, 2013). When dealing with saline soils, EC$_a$ measurements can be used as proxy for soil salinity (Lobell et al., 2010; Wu, Al-Shafie, et al., 2014; Ding & Yu, 2014), as the more ions in the soil solution, the more conductive the soil (Corwin & Lesch, 2013). A total of 267 soil sampling locations (each covering ca 2 × 2 m of soil) were selected from the 22 fields. The sampling schemes (one for each field) were designed in order to best represent the spatial variations of EC$_a$ (and, thus, of soil salinity), using a Response Surface Sampling Design (RSSD) algorithm (Lesch, 2005).

At each of the 267 soil sampling locations, the root-zone (0–1.2 m) salinity was measured as electrical conductivity of the soil saturation extract, i.e., EC$_e$, dS m^{-1} (U.S. Salinity Laboratory Staff, 1954). The EC$_a$ readings were then calibrated (R^2 = 0.93) against the EC$_e$ measurements (Scudiero, Skaggs, & Corwin, 2014). Salinity estimates (EC$_e^*$, dS m^{-1}) for the 22 fields were obtained from the EC$_a$–EC$_e$ relationships. Kriging with 30 × 30 m block support was used to interpolate the point EC$_e^*$ data onto a regular 30 × 30 m grid (Lobell et al., 2010), using isotropic exponential semivariograms in ArcMap 10.1 (ESRI, Redlands, CA, USA). The interpolation resulted in 5891, 30 × 30 m, EC$_e^*$ estimates. To reduce bias in the L7–EC$_e^*$ due to field edge effect, the L7 pixels at the field margins were removed from the ground-truth dataset (i.e., 608 pixels). The exclusion of these field edge pixels is discussed in Section 4.3 ("On Field Edge Effect"). The average, minimum, and maximum EC$_e^*$ were of 7.55, 0.01, and 35.2 dS m^{-1} (Scudiero, Skaggs, & Corwin, 2014).

3.3. Soil and environmental covariates

When studying the reasons for the spatio-temporal variability of the L7-soil salinity relationships over the WSJV, Scudiero, Skaggs, and Corwin (2014) indicated that those relationships changed, between fields, according to soil texture and, between years, according to yearly rainfall and yearly average minimum temperature. Moreover, the research of Lobell et al. (2010) in the Red River Valley, USA, and of Zhang et al. (2015) in the Yellow River Delta, China, clearly shows that cropped and fallow/wasteland (i.e., a mix of halophytic plants and bare-soil) surface reflectance show remarkably different relationships with soil salinity.

Soil texture data were obtained from the Natural Resources Conservation Service (NRCS) Soil Survey Geographic database (SSURGO). SSURGO divides the land surface into elements called map units. Map units encompass more than one component (soil type), each having their own representative soil profile. Within map units, components are not spatially located; they are represented only in terms of their estimated percent coverage of the map unit. According to NRCS (http://www.nrcs.usda.gov/wps/portal/nrcs/detail/soils/survey/?cit=nrcs142p2_054236), field investigations and data collection are carried out in sufficient detail to name map units and to identify accurately and consistently areas of about 1 ha. The SSURGO data corresponding to our 22 fields sites were all collected in surveys having a sampling intensity appropriate for 1:24,000 maps. To determine a single numerical value for the sand, silt, and clay percentages (%) of each pixel, we calculated profile depth-average sand, silt, and clay values for each major soil component of corresponding map unit, and then set the pixel value to be equal to the component-percentage-weighted average of those values. So, for example, if the jth pixel falls in a SSURGO map unit having N major components, the silt content (%) for that pixel is:

$$\text{SILT}_j = \sum_{k=1}^{N} \left[\frac{x_k}{X} \sum_{i=1}^{M_k} \frac{s_i \Delta z_i}{Z_k} \right] \tag{2}$$

where x_k is the percentage of the map unit covered by the kth soil component, $X = \sum_{k=1}^{N} x_k$, M_k is the number of soil layers in the kth soil component, s_i is the silt percentage in the ith layer, Δz_i is the thickness of the ith layer, and Z_k is the total depth the kth soil component.

The meteorological data was obtained from the Climate Group from Oregon State University (Corvallis, OR, USA) through their Parameter-elevation Relationships on Independent Slopes Model (PRISM) (Daly et al., 2008), which provides monthly meteorological data on a 4×4 km cell support. Yearly total rainfall (mm) and average minimum temperature (°C) were used, at each pixel (j) from to the year with maximum CRSI.

Crop data since 2007 is available for the USA at the CropScape database (Han et al., 2012), which presents an easily accessible version of the Cropland Data Layer (Boryan, Yang, Mueller, & Craig, 2011). The pixels with maximum CRSI were cultivated with alfalfa (*Medicago sativa* L.), cotton (*Gossypium* sp.), wheat (*Triticum aestivum* L.), maize (*Zea mays* L.), safflower (*Carthamus tinctorius* L.), with mixes of forage grass communities (i.e., pasture), or left as fallow. About 16% of the pixels were fallow, whereas the remaining pixels were cropped.

3.4. Model formulation, calibration, and validation

The simplest predictive model for soil salinity would be based on the linear relationship between CRSI and soil salinity. To improve upon that model, we evaluated alternative formulations that additionally utilized soil-environmental covariates. The specific model formulations considered are given in the results section, but in general the soil type and meteorological covariates were regarded as additional (to CRSI) explanatory variables of a multiple linear regression having EC_e^* as the dependent variable. The crop covariate was regarded as a factor having a direct effect on the CRSI values, as seen in previous studies by Lobell et al. (2010) and Zhang et al. (2015). Therefore, when the crop information was included, CRSI was characterized by an additional regression parameter, whether the target pixel was cropped or fallow.

In spatial datasets, neighboring records tend to be very similar, therefore, using traditional cross-validation (CV) methods can lead to almost identical data values in the training and the validation datasets, returning biased predictions (Ruß & Brenning, 2010) with overly optimistic low errors (Ruß & Brenning, 2010; Brenning, 2012). In order to assure spatial independence between training and validation datasets, the salinity assessment models were cross-validated with a leave-one-field-out (*lofo*) procedure. The procedure was developed after the research of Ruß and Brenning (2010), who proposed a special case of k-fold CV, in which the dataset were divided into spatially independent clusters, each representing a fold in the CV procedure. In the *lofo*, each field represents an independent spatial group. The *lofo* procedure is expected to have less optimistic validation errors than a standard cross-validation procedure. Twenty-two iterations were carried out: one field was retained for validation at each iteration, whereas the remaining 21 fields were used to train the compared salinity prediction models. The validation results across models were compared by testing the distributions of the absolute errors (AE) with the non-parametric Kruskal-

Wallis rank test (Kruskal & Wallis, 1952). Comparisons were carried out on the validation predictions globally, and within the 0–2 (non-saline), 2–4 (slightly saline), 4–8 (moderately saline), 8–16 (strongly saline), and >16 (extremely saline) dS m^{-1} salinity intervals.

4. Results and discussion

4.1. Assessing soil salinity with ETM + reflectance and soil-environmental covariates

The linear relationship of CRSI with soil salinity (Eq. (3), R^2 = 0.564) is used as a reference to evaluate the performance of models employing additional explanatory variables (Table 1).

$$EC_{e,j}^* = 99.70 - 111.81 \times CRSI_j + \varepsilon_j \tag{3}$$

In Eq. (3), ε (dS m^{-1}) is the random error component at each location j. In this equation as well as the regressions presented below, the dimensions of the numerical coefficients are defined implicitly by the dimensions of the response and predictor variables (Table 1). Eq. (3) (and the other presented regressions) had significant (p > 0.01) ANOVA F-test and coefficients (t-test). All the linear regression assumptions (for all equations) were also verified. Fig. 2 shows the observed and predicted salinity values from the corresponding validation datasets (R^2 = 0.483). The validation MAE was 3.55 dS m^{-1} (Table 2). In the non-, slightly, moderately, strongly, and extremely saline soils, validation MAEs were 2.74, 2.55, 3.40, 4.03, 6.89 dS m^{-1}, respectively (Table 2). The MAEs for the field average, minimum, and maximum salinity predicted with Eq. (3) were 3.19, 2.93, and 3.35 dS m^{-1}, respectively (Table 3). Table 3 gives additional statistics and parameters (Pearson's r, slope, intercept) for the observed-predicted salinity relationships evaluated on a "per-field" basis (i.e. in terms of field averages, minimums, and maximums).

The observations of Scudiero, Skaggs, and Corwin (2014) and the salinity assessment models presented by Taghizadeh-Mehrjardi et al. (2014) indicate that incorporating geo-morphological factors (e.g., soil texture, micro-elevation) into remote sensing data-based models can improve their accuracy. The introduction of a soil texture covariate (i.e., percent of silt) significantly improved the global goodness-of-fit of the L7–EC$_e^*$ relationship, with R^2 = 0.583:

$$EC_{e,j}^* = 103.28 - 112.64 \times CRSI_j - 0.09 \times SILT_j + \varepsilon_j. \tag{4}$$

However, the validation R^2 (Table 1) of Eq. (4) was worse compared to Eq. (3), and so were the global and by-salinity-class MAE values (Table 2). The per-field predictions were also worse when SSURGO silt values was used as explanatory variable. It is fair to conclude that SSURGO textural information is too coarse to be used at the ETM + spatial resolution. In fact, at the sub-field scale, soil texture in the WSJV generally shows sizeable variations at the sub-field scale. Most likely, the use of finer resolution soil data could improve the salinity predictions considerably. When using the measured textural properties (Scudiero, Skaggs, & Corwin, 2014) at the 267 sampling locations as an explanatory co-

Table 1
Coefficients of determination (R^2) between Eqs. (3), (4), (5), (6), and (7) and ground-truth salinity: *i*) Observed = R^2 for fit to entire dataset; and *ii*) Validation = R^2 for the 22 leave-one-field-out cross-validations.

Model[a]		Observed R^2	Validation R^2
Eq. (3)	$EC_{e,j}^* = 99.70 - 111.81 \times CRSI_j + \varepsilon_j$	0.564	0.483
Eq. (4)	$EC_{e,j}^* = 103.28 - 112.64 \times CRSI_j - 0.09 \times SILT_j + \varepsilon_j$	0.583	0.475
Eq. (5)	$EC_{e,j}^* = 62.88 - 113.35 \times CRSI_j + 0.02 \times RAIN_j + 2.00 \times TEMP_j + \varepsilon_j$	0.637	0.486
Eq. (6)	$EC_{e,j}^* = 91.39 + \beta_{crop} \times CRSI_j + \varepsilon_j$	0.601	0.512
Eq. (7)	$EC_{e,j}^* = 26.3 + \beta_{crop} \times CRSI_j + 0.025 \times RAIN_j + 3.35 \times TEMP_j + \varepsilon_j$	0.728	0.611

[a] EC_e^*, ground-truth soil salinity (dS m^{-1}); j, Landsat 7 pixel location; CRSI, canopy response salinity index (unitless); SILT, soil silt percentage, RAIN, yearly total rainfall (mm); TEMP, yearly average minimum temperature (°C); *crop*, field management type (i.e., cropped or fallow); and ε, random error component (dS m^{-1}).
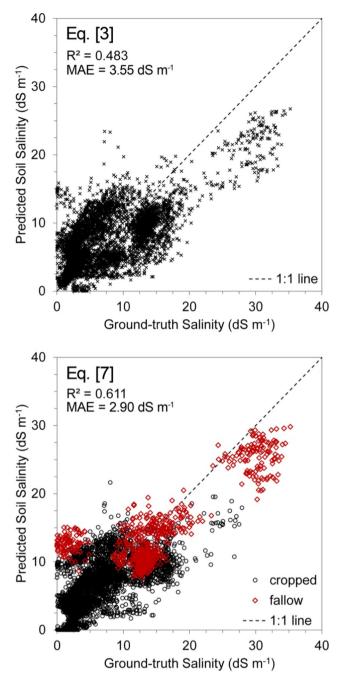
Table 3
Summary statistics for *lofo* cross-validation evaluated on a per-field basis.

Model	Per-field salinity	Pearson's r	Slope	Intercept	MAE (dS m^{-1})
Eq. (3)	AVE	0.82	0.59	2.61	3.19
	MIN	0.76	0.47	1.66	2.93
	MAX	0.87	0.66	3.41	3.35
Eq. (4)	AVE	0.81	0.60	2.30	3.34
	MIN	0.80	0.54	1.08	2.90
	MAX	0.84	0.66	3.34	3.50
Eq. (5)	AVE	0.85	0.65	2.21	2.94
	MIN	0.76	0.50	1.18	3.01
	MAX	0.88	0.75	2.79	3.09
Eq. (6)	AVE	0.84	0.63	2.36	3.06
	MIN	0.77	0.50	1.59	2.86
	MAX	0.89	0.70	3.05	3.18
Eq. (7)	AVE	0.89	0.71	1.90	2.46
	MIN	0.87	0.61	1.37	2.25
	MAX	0.87	0.72	2.62	3.09

variable, there was a remarkable improvement of the validation R^2 ($+6.6\%$) and MAE (-6.2%) compared to those of the simple linear CRSI- EC_e^* model. The SSURGO texture dataset could be of great help, however, in salinity assessment studies carried out at much coarser resolutions.

The PRISM meteorological data also does not match the spatial resolution of the ETM+ reflectance. However, it is safe to assume that there is little to no spatial variability in the monthly rainfall and temperature data within a 16 km^2 cell (Scudiero, Skaggs, & Corwin, 2014; Tardivo, 2014). Indeed, the difference in resolution between L7 and PRISM data did not prove to be an issue. The addition of RAIN and TEMP as independent variables (Eq. (5)) improved the explained variance of Eq. (3) by 13.1% ($R^2 = 0.637$).

$$EC_{e,j}^* = 62.88 - 113.35 \times CRSI_j + 0.02 \times RAIN_j + 2.00 \times TEMP_j + \varepsilon_j \quad (5)$$

The *lofo* validation errors of Eq. (5) with validation $R^2 = 0.486$ were slightly improved with respect to Eq. (3). The global MAE was 3.53 dS m^{-1} and 2.76, 2.34, 3.13, 4.45, and 6.34 dS m^{-1} in the non-, slightly, moderately, strongly, and extremely saline soils, respectively.

The use of different regression coefficients for CRSI according to crop type (Eq. (6)) returned a $R^2 = 0.601$, consistent with the observations of Lobell et al. (2010) and Zhang et al. (2015). Eq. (6) increased the explained variance by 6.7% with respect to Eq. (3):

$$EC_{e,j}^* = 91.39 + \beta_{crop} \times CRSI_j + \varepsilon_j \quad (6)$$

where β_{crop} was -102.53 and -97.96 for cropped and fallow soils, respectively. Eq. (6) improved validation performance both at the global scale ($R^2 = 0.512$, MAE $= 3.45$ dS m^{-1}) and, generally, over the five salinity ranges (Table 2).

Fig. 2. Relationships between observed ground-truth salinity (EC_e^*) and validation predictions using Eqs. (3) and (7). The coefficients of determination (R^2) and mean absolute error (MAE) for the two models are reported in the figure.

Table 2
Performance of the validation predictions for Eqs. (3), (4), (5), (6), and (7). Letters adjacent to the mean absolute errors values indicate significant (p < 0.05) differences, between different models, in the absolute error distribution according to the Kruskal–Wallis rank test.

Model	Validation						
	R^2	Mean absolute error (dS m^{-1})					
		Entire dataset	Non-saline soils (0–2 dS m^{-1})	Slightly saline soils (2–4 dS m^{-1})	Moderately saline soils (4–8 dS m^{-1})	Strongly saline soils (8–16 dS m^{-1})	Extremely saline soils (>16 dS m^{-1})
Eq. (3)	0.483	3.55 bc	2.74 a	2.55 c	3.40 bc	4.03 b	6.89 bc
Eq. (4)	0.475	3.62 c	2.83 b	2.94 d	3.48 c	3.89 b	6.68 b
Eq. (5)	0.485	3.53 bc	2.76 ab	2.34 b	3.13 b	4.45 c	6.34 b
Eq. (6)	0.512	3.45 b	2.71 a	2.53 c	3.37 b	3.89 b	6.26 ab
Eq. (7)	0.611	2.90 a	2.94 c	2.12 a	2.35 a	3.23 a	5.64 a

Joining Eqs. (5) and (6) the following model was derived:

$$EC^*_{e,j} = 26.3 + \beta_{crop} \times CRSI_j + 0.025 \times RAIN_j + 3.35 \times TEMP_j + \varepsilon_j \quad (7)$$

where β_{crop} was -100.76 and -93.40 for cropped and fallow soils, respectively. With a $R^2 = 0.732$, Eq. (7) improves Eq. (3) by 24.8%. The *lofo* CV returned a validation $R^2 = 0.611$ (Fig. 2) and global MAE = 2.90 dS m^{-1}. In the non-, slightly, moderately, strongly, and extremely saline soils, the validation MAEs were 2.94, 2.12, 2.35, 3.23, and 5.64 dS m^{-1}, respectively. The per-field average, minimum, and maximum salinity predictions were also remarkably improved in comparison to those of Eq. (3). Fig. 2 shows how the use of separate β_{crop} coefficients for cropped and fallow soils in Eq. (7) significantly improved the soil salinity predictions, compared to Eq. (3). Similar to what was seen by Zhang et al. (2015), when salinity is <10 dS m^{-1} one should expect big prediction errors for fallow soils, probably because halophyte growth at those salinity levels is limited (Zhang et al., 2011): the competition between weed species is likely to be higher as the salinity stress level is not extreme. In this salinity range, fallow fields are likely to host multiple weed species. Each species would most likely colonize the field in clusters (Cardina, Johnson, & Sparrow, 1997) and be characterized by its own light adsorption properties (e.g., due to different phenology and physiology). This scenario would add noise to the salinity prediction model, reducing the effect of salinity on CRSI determination.

In addition to the goodness-of-fit scores (e.g., validation R^2, validation MAE) of a model, one should consider how uncertain the validation predictions are in comparison to the model prediction interval (Minasny, 2013). In order to better understand the prediction power of different model formulations, the absolute error (AE) frequency distribution can be studied. In Fig. 3, the *lofo* predictions of Eqs. (3) and (7) are compared both over the global relationship and by salinity class. This type of analysis ascertains the uncertainty of the validation predictions between different salinity assessment models. In particular, the use of the meteorological and crop covariates in Eq. (7) lead to reduced prediction uncertainties, compared to Eq. (3), in the slightly, moderately, strongly, and extremely saline soils. Some sensitivity is lost, however, in the non-saline soils. Additionally, Fig. 3 shows the importance of extreme prediction errors in the model selection procedure. Although predictions of non-saline soils were more accurate in Eq. (3) than Eq. (7) (Table 2), in Eq. (3) 30% of the AEs for non saline soils are >4 dS m^{-1}, whereas Eq. (7) has 19%.

In this paper, and in other published studies (Lobell et al., 2010; Zhang et al., 2015; Wu, Al-Shafie, et al., 2014; Taghizadeh-Mehrjardi et al., 2014; Ding & Yu, 2014; Hamzeh et al., 2013), a considerable portion of the variance (specific to each ground-truth salinity dataset) is not explained. When using canopy reflectance, one should always keep in mind that the VI are indirectly measuring crop health/status by simultaneously recording information on multiple parameters (Mulla, 2013), including leaf area index, biomass, and chlorophyll content. Therefore, decreases of reflectance performances can be due to many factors, including biotic and abiotic stress sources. This paper highlights the importance of using multi-year reflectance to assess soil salinity. In particular, the yearly average highlights features that are stable in time, such as salinity (Lobell et al., 2010), whereas the multi-year maximum VI further masks the effects of other stress types (Wu, Al-Shafie, et al., 2014). Nevertheless, abrupt changes in agronomical practices (e.g., shifting from
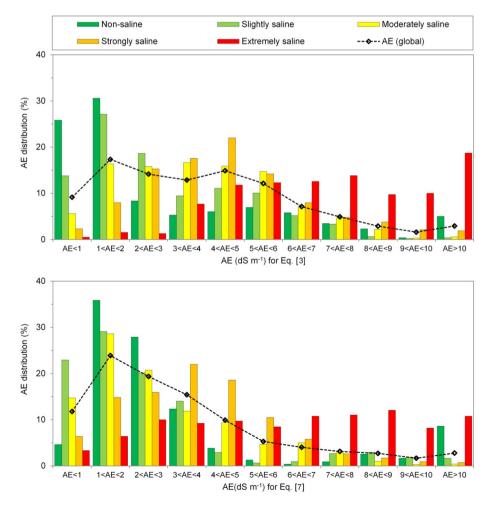

Fig. 3. Frequency distribution for the absolute errors (AE) of the validation predictions for a) Eq. (3) and b) Eq. (7). The AE distributions are shown, with a dashed line, for the entire dataset and with bars for five selected salinity classes: 0–2 (non-saline), 2–4 (slightly saline), 4–8 (moderately saline), 8–16 (strongly saline), and above 16 (extremely saline) dS m^{-1}.

cultivated to fallow), which generally result in fast changes of root-zone salinity (Corwin, 2014), may increase the uncertainty of salinity estimation of the presented approach. Additionally, salinity is not the only abiotic stress fairly stable in time. For example, sodicity in non-saline soils is an issue that can bias the salinity assessment models. Indeed, several portions of the WSJV are characterized by non- and slightly saline soils having high pH values (pH > 9) suggesting the presence of sodic soils (Scudiero, Skaggs, et al., 2014). Additionally, halophytic weed communities have salinity tolerances that vary from species to species (Flowers & Colmer, 2008), the transition from vegetated and bare-soil fallow land could be a major reason for uncertainty in the predictions over vegetated, extremely saline soils.

A possible issue could arise when trying to assess soil salinity at much greater scales (e.g., California-, USA-, and World-wide) than the one investigated. The ability of remote sensing data to capture soil–plant relationships changes according to geographical context (Allbed & Kumar, 2013; Hadjimitsis et al., 2010) due to a number of factors, including lithologic and meteorological settings. If such changes in soil salinity accuracy of multi-year ETM + canopy reflectance and soil/environmental covariates are of a strong non-linear nature, a single linear model (e.g., Eq. (7)) would not be reliable if the region were too big. This matter should be further investigated in future research, as there is much need for state-, national-, and global-scale salinity inventories.

4.2. On spatial cross-validation

The *lofo* spatial CV methodology proposed here is for regional-scale salinity models using ground truth observations from different fields. Consistent with the observations of Ruß and Brenning (2010) for a field-scale spatial CV, the *lofo* CV is less optimistic than traditional CV methods. Indeed, using a classic *k*-fold CV (with *k* = 22) for Eq. (7) outputs a better observed-predicted relationship, with $R^2 = 0.679$ (11% greater than *lofo*), and MAE = 2.53 dS m^{-1} (13% lower than *lofo*). Similar biased validation outputs were observed in the non-, slight, moderate, strong, and extreme salinity intervals, with prediction MAEs being, respectively, 12, 9, 10, 19, and 9% more optimistic with the traditional *k*-fold than with the *lofo*, and in the per-field scores, with more optimistic MAEs for field average, minimum, and maximum salinity (9, 15, and 13%, respectively).

4.3. On field edge effect

The assessment model in this case study was built over ground-truth data not including the field edges. It is well known that plant performances at the field edges (i.e., "headlands") are reduced compared to the rest of the field (i.e., lower VI values), due to a variety of factors (Sparkes, Jaggard, Ramsden, & Scott, 1998), including: compaction from traffic on field edges, reduced water content due to field settings, intensified weed and insect pressure, and different evapotranspiration conditions. Additionally, the resolution of L7 does not allow distinguishing between actual field edges and features that can be found along the edges of the fields (e.g., roads, water canals, etc).

Table 4 reports the statistics on salinity assessment over the 608 field-edge pixels. When soil salinity was predicted using Eq. (7)

calibrated over the full-field dataset, ca. 70% of the pixels returned an overestimated salinity values. Clearly, and consistent with the literature (Sparkes et al., 1998), crop performance at the field edges is lower than that observed over the rest of the field, regardless of the influence of soil salinity. If shape files with the field borders are not available, it is therefore advisable to not include field edges in the calibration dataset. Alternatively, a buffer area can be calculated for field edges and the salinity assessment models can be computed with different parameter values for the two cases.

4.4. A note on the evaluation of salinity assessment models

When trying to describe the relationships between canopy reflectance and soil salinity, linear regression methods are by far the most popular in recently published studies (e.g., Lobell et al., 2010; Zhang et al., 2015; Wu, Al-Shafie, et al., 2014; Taghizadeh-Mehrjardi et al., 2014). However, there are several limitations to this approach that should be considered when building the salinity assessment model(s) and when presenting the results.

The R^2 and other goodness-of-fit measurements (e.g., MAE, RMSE, and Ratio of Performance to Deviation) are a function of the range and variance of the ground-truth observations (Ji & Peters, 2007; Minasny, 2013; Achen, 1982). They should be used solely to compare different models nested on the same dependent variable dataset, not to compare goodness-of-fit across studies using different databases, as is done too often in the literature (Hyndman & Koehler, 2006). As shown by Scudiero, Skaggs, and Corwin (2014), it is reasonable to expect a higher R^2 when high salinity values are included in the model. High R^2 values can be obtained with fairly good predictions for non-productive, extremely saline soils (e.g., $EC_e > 50$ dS m^{-1}), but with massive errors in the $EC_e < 16$ dS m^{-1} salinity ranges, where crops can grow (Wu, Al-Shafie, et al., 2014; Nawar et al., 2015; Taghizadeh-Mehrjardi et al., 2014; Allbed et al., 2014; Yang et al., 2015). In other words, a $\pm$ 10 dS m^{-1} prediction error over a 100 dS m^{-1} soil would still qualify a soil as "wasteland"/"uncultivable", whereas the same prediction error over a 10 dS m^{-1} soil would lead to highly erroneous/uncertain decision-making. Greater attention should be given to building models with low prediction errors in the cultivable ranges of soil salinity.

5. Conclusions

We explored the potentials and limitations of developing regional-scale soil salinity maps using multi-year ETM + CRSI data. For the first time, a reliable (i.e., low cross-validation errors) regional-scale salinity model is presented in the environmentally and agronomically relevant ranges of soil salinity ($EC_e < 20$ dS m^{-1}). Alone, CRSI explained 56% of the variance of the measured soil salinity spatial variability over 22 fields in the western San Joaquin Valley. Including information for crop type and meteorological data in the model (Eq. (7)) remarkably improved the accuracy and precision of the EC_e^* predictions (fitted $R^2 = 0.728$, cross-validation $R^2 = 0.611$), with greater accuracy obtained over the entire dataset, in the different salinity classes, and at the per-field level. The results also suggest that the prediction power of the

Table 4
Use of Eq. (7) over the 608 Landsat 7 pixels at the field edges: (1) extrapolated predictions using the model parameters calibrated over the full-fields dataset; (2) model re-calibration using edge pixels data; and (3) leave-one-field-out (*lofo*) cross-validation for the edge pixels.

Scenario	R^2	Mean absolute error (dS m^{-1})					
		Entire dataset	Non-saline soils (0–2 dS m^{-1})	Slightly saline soils (2–4 dS m^{-1})	Moderately saline soils (4–8 dS m^{-1})	Strongly saline soils (8–16 dS m^{-1})	Extremely saline soils (>16 dS m^{-1})
(1) Full-fields calibration applied to edge pixels	0.361	4.35	2.75	4.81	4.69	4.79	2.88
(2) Re-calibration to edge pixel data	0.476	3.17	1.76	2.78	2.43	4.56	6.40
(3) *lofo* CV for edge pixels	0.454	3.36	1.75	3.55	3.20	3.50	9.64

salinity assessment models would be further improved if high resolution ancillary data on soil texture were available.

Future research will focus on the creation and independent validation of salinity maps for the San Joaquin Valley and, possibly, for other sensible agricultural areas in California, such as the Coachella and Imperial Valleys. To map salinity over large scales, a mosaic of different tiles of Landsat ETM + is needed. Fortunately, this service is available from USGS, thanks to the Web-enabled Landsat data (WELD) project (Roy et al., 2010). Once the regional scale maps are made, the long term anthropological (e.g., management) and natural (e.g., drought, climate changes) effects on soil quality can be assessed, by comparing the remote sensing estimations with past salinity inventories.

Acknowledgments

References

Achen, C.H. (1982). Interpreting and using regression. *Sage University Paper Series on Quantitative Application in the Social Sciences 07–001.* Beverly Hills: Sage Publications (85 pp.).

Aldabaa, A.A.A., Weindorf, D.C., Chakraborty, S., Sharma, A., & Li, B. (2015). Combination of proximal and remote sensing methods for rapid soil salinity quantification. *Geoderma, 239,* 34–46.

Allbed, A., & Kumar, L. (2013). Soil salinity mapping and monitoring in arid and semi-arid regions using remote sensing technology: a review. *Advances in Remote Sensing, 2,* 373–385.

Allbed, A., Kumar, L., & Sinha, P. (2014). Mapping and modelling spatial variation in soil salinity in the Al Hassa Oasis based on remote sensing indicators and regression techniques. *Remote Sensing, 6,* 1137–1157.

Backlund, V.L., & Hoppes, R.R. (1984). Status of soil salinity in California. *California Agriculture, 38,* 8–9.

Boryan, C., Yang, Z., Mueller, R., & Craig, M. (2011). Monitoring US agriculture: the US department of agriculture, national agricultural statistics service, cropland data layer program. *Geocarto International, 26,* 341–358.

Brenning, A. (2012). Spatial cross-validation and bootstrap for the assessment of prediction rules in remote sensing: The R package sperrorest. *IEEE International Geoscience and Remote Sensing Symposium, IGARSS 2012, 23–27 July 2012* (pp. 5372–5375).

Brown, J.J., Cybulska, I., Chaturvedi, T., & Thomsen, M.H. (2014). Halophytes for the Production of Liquid Biofuels. In M.A. Khan, B. Böer, M. Öztürk, T.Z. Al Abdessalaam, M. Clüsener-Godt, & B. Gul (Eds.), *Sabkha Ecosystems: Volume IV: Cash Crop Halophyte and Biodiversity Conservation* (pp. 67–72). The Netherlands: Springer.

Cardina, J., Johnson, G.A., & Sparrow, D.H. (1997). The nature and consequence of weed spatial distribution. *Weed Science, 45,* 364–373.

Cone, T. (1997). The vanishing valley. *San Jose Mercury News Magazine, June 29* (pp. 9–15).

Corwin, D.L. (2014). Field-scale monitoring of the long-term impact and sustainability of drainage water reuse using ECa-directed soil sampling. *ASA, CSA, and SSSA Annual Meeting, Long Beach, CA, USA, 1–4 November 2014.*

Corwin, D.L., & Lesch, S.M. (2013). Protocols and guidelines for field-scale measurement of soil salinity distribution with ECa-directed soil sampling. *Journal of Environmental and Engineering Geophysics, 18,* 1–25.

Corwin, D.L., Lesch, S.M., Oster, J.D., & Kaffka, S.R. (2006). Monitoring management-induced spatio–temporal changes in soil quality through soil sampling directed by apparent electrical conductivity. *Geoderma, 131,* 369–387.

Corwin, D.L., Lesch, S.M., Oster, J.D., & Kaffka, S.R. (2008). Short-term sustainability of drainage water reuse: spatio-temporal impacts on soil chemical properties. *Journal of Environmental Quality, 37,* 8–24.

Daly, C., Halbleib, M., Smith, J.I., Gibson, W.P., Doggett, M.K., Taylor, G.H., et al. (2008). Physiographically sensitive mapping of climatological temperature and precipitation across the conterminous United States. *International Journal of Climatology, 28,* 2031–2064.

Ding, J., & Yu, D. (2014). Monitoring and evaluating spatial variability of soil salinity in dry and wet seasons in the Werigan–Kuqa Oasis, China: remote sensing and electromagnetic induction instruments. *Geoderma, 235,* 316–322.

Eldeiry, A., & Garcia, L.A. (2008). Detecting soil salinity in alfalfa fields using spatial modeling and remote sensing. *Soil Science Society of America Journal, 72,* 201–211.

Flowers, T.J., & Colmer, T.D. (2008). Salinity tolerance in halophytes. *New Phytologist, 179,* 945–963.

Furby, S., Caccetta, P., & Wallace, J. (2010). Salinity monitoring in Western Australia using remotely sensed and other spatial data. *Journal of Environmental Quality, 39,* 16–25.

Ghassemi, F., Jakeman, A.J., & Nix, H.A. (1995). *Salinisation of land and water resources: human causes, extent, management and case studies.* Wallingford, Oxon, UK: CAB International, 526.

Hadjimitsis, D.G., Papadavid, C., Agapiou, A., Themistocleous, K., Hadjimitsis, M., Retalis, A., et al. (2010). Atmospheric correction for satellite remotely sensed data intended for agricultural applications: impact on vegetation indices. *Natural Hazards and Earth System Sciences, 10,* 89–95.

Hamzeh, S., Naseri, A., AlaviPanah, S., Mojaradi, B., Bartholomeus, H.M., Clevers, J.G., et al. (2013). Estimating salinity stress in sugarcane fields with spaceborne hyperspectral vegetation indices. *International Journal of Applied Earth Observation and Geoinformation, 21,* 282–290.

Han, W., Yang, Z., Di, L., & Mueller, R. (2012). CropScape: a web service based application for exploring and disseminating US conterminous geospatial cropland data products for decision support. *Computers and Electronics in Agriculture, 84,* 111–123.

Howitt, R., Medellín-Azuara, J., MacEwan, D., Lund, J., & Sumner, D. (2014). *Economic analysis of the 2014 drought for California agriculture.* Davis, CA: UC–Davis Center for Watershed Sciences (Online at https://watershed.ucdavis.edu/files/biblio/DroughtReport_23July2014_0.pdf).

Huete, A., Didan, K., Miura, T., Rodriguez, E.P., Gao, X., & Ferreira, L.G. (2002). Overview of the radiometric and biophysical performance of the MODIS vegetation indices. *Remote Sensing of Environment, 83,* 195–213.

Hyndman, R.J., & Koehler, A.B. (2006). Another look at measures of forecast accuracy. *International Journal of Forecasting, 22,* 679–688.

Ivits, E., Cherlet, M., Tóth, T., Lewińska, K., & Tóth, G. (2011). Characterisation of productivity limitation of salt-affected lands in different climatic regions of Europe using remote sensing derived productivity indicators. *Land Degradation & Development, 24,* 438–452.

Ji, L., & Peters, A.J. (2007). Performance evaluation of spectral vegetation indices using a statistical sensitivity function. *Remote Sensing of Environment, 106,* 59–65.

Kruskal, W.H., & Wallis, W.A. (1952). Use of ranks in one-criterion variance analysis. *Journal of the American Statistical Association, 47,* 583–621.

Lal, R., Iivari, T., & Kimble, J.M. (2004). *Soil degradation in the United States: extent, severity, and trends.* Boca Raton, FL, USA: CRC Press.

Lesch, S. (2005). Sensor-directed response surface sampling designs for characterizing spatial variation in soil properties. *Computers and Electronics in Agriculture, 46,* 153–179.

Letey, J., & Dinar, A. (1986). Simulated crop-water production functions for several crops when irrigated with saline waters. *Hilgardia, 54,* 1–32.

Lobell, D.B. (2010). Remote sensing of soil degradation: introduction. *Journal of Environmental Quality, 39,* 1–4.

Lobell, D.B., Lesch, S.M., Corwin, D.L., Ulmer, M.G., Anderson, K.A., Potts, D.J., et al. (2010). Regional-scale assessment of soil salinity in the Red River Valley using multi-year MODIS EVI and NDVI. *Journal of Environmental Quality, 39,* 35–41.

Lobell, D.B., Ortiz-Monasterio, J.I., Gurrola, F.C., & Valenzuela, L. (2007). Identification of saline soils with multiyear remote sensing of crop yields. *Soil Science Society of America Journal, 71,* 777–783.

Masek, J.G., Vermote, E.F., Saleous, N.E., Wolfe, R., Hall, F.G., Huemmrich, K.F., et al. (2006). A Landsat surface reflectance dataset for North America, 1990–2000. *IEEE Geoscience and Remote Sensing Letters, 3,* 68–72.

Metternicht, G., & Zinck, J. (2003). Remote sensing of soil salinity: potentials and constraints. *Remote Sensing of Environment, 85,* 1–20.

Miller, B.A., Koszinski, S., Wehrhan, M., & Sommer, M. (2015). Impact of multi-scale predictor selection for modeling soil properties. *Geoderma, 239,* 97–106.

Minasny, B. (2013). Why you don't need to use RPD. *Pedometron, 33,* 14–15.

Mougenot, B., Pouget, M., & Epema, G. (1993). Remote sensing of salt affected soils. *Remote Sensing Reviews, 7,* 241–259.

Mulla, D.J. (2013). Twenty five years of remote sensing in precision agriculture: key advances and remaining knowledge gaps. *Biosystems Engineering, 11,* 358–371.

Nawar, S., Buddenbaum, H., & Hill, J. (2015). Digital mapping of soil properties using multivariate statistical analysis and ASTER data in an arid region. *Remote Sensing, 7,* 1181–1205.

Rouse, J., Haas, R., Schell, J., & Deering, D. (1973). Monitoring vegetation systems in the Great Plains with ERTS. *Third ERTS Symposium. NASA SP-351* (pp. 309–317).

Roy, D.P., Ju, J., Kline, K., Scaramuzza, P.L., Kovalskyy, V., Hansen, M., et al. (2010). Web-enabled Landsat Data (WELD): Landsat ETM composited mosaics of the conterminous United States. *Remote Sensing of Environment, 114,* 35–49.

Ruß, G., & Brenning, A. (2010). Data mining in precision agriculture: management of spatial information. In E. Hüllermeier, R. Kruse, & F. Hoffmann (Eds.), *Computational intelligence for knowledge-based systems design. Lecture Notes in Computer Sciences, 6178.* (pp. 350–359). Heidelberg, Germany: Springer.

Samuel-Rosa, A., Heuvelink, G., Vasques, G., & Anjos, L. (2015). Do more detailed environmental covariates deliver more accurate soil maps? *Geoderma, 243,* 214–227.

Scudiero, E., Skaggs, T.H., & Corwin, D.L. (2014a). Regional Scale Soil Salinity Evaluation Using Landsat 7, Western San Joaquin Valley, California, USA. *Geoderma Regional, 2–3,* 82–90.

Scudiero, E., Teatini, P., Corwin, D.L., Ferro, N.D., Simonetti, G., & Morari, F. (2014b). Spatiotemporal response of maize yield to edaphic and meteorological conditions in a saline farmland. *Agronomy Journal, 106,* 2163–2174.

Skaggs, T., Anderson, R., Corwin, D., & Suarez, D. (2014). Analytical steady-state solutions for water-limited cropping systems using saline irrigation water. *Water Resources Research, 12,* 9656–9674.

Sparkes, D., Jaggard, K., Ramsden, S., & Scott, R. (1998). The effect of field margins on the yield of sugar beet and cereal crops. *Annals of Applied Biology, 132,* 129–142.

Taghizadeh-Mehrjardi, R., Minasny, B., Sarmadian, F., & Malone, B. (2014). Digital mapping of soil salinity in Ardakan region, central Iran. *Geoderma, 213,* 15–28.

Tanji, K.K., & Wallender, W.W. (2012). Nature and extent of agricultural salinity and sodicity. In W.W. Wallender, & K.K. Tanji (Eds.), *Agricultural Salinity Assessment and Management. Reston, VA, USA: ASCE Manuals and Reports on Engineering Practices No. 71.* (pp. 10–25). Reston, VA, USA: ASCE.

Tardivo, G. (2014). Spatial and time correlation of thermometers and pluviometers in a weather network database. *Theoretical and Applied Climatology,* http://dx.doi.org/10.1007/s00704-014-1148-5.

U.S. Salinity Laboratory Staff (1954). *USDA Handbook no. 60. Diagnosis and improvement of saline and alkali soils.* Washington, D.C.: U.S. Government Printing Office.

Wu, W., Al-Shafie, W., Mhaimeed, A., Ziadat, F., Nangia, V., & Payne, W. (2014a). Soil salinity mapping by multiscale remote sensing in Mesopotamia, Iraq. *IEEE Journal of Selected Topics in Applied Earth Observations and Remote Sensing, 7,* 4442–4452.

Wu, W., Mhaimeed, A.S., Al-Shafie, W.M., Ziadat, F., Dhehibi, B., Nangia, V., et al. (2014b). Mapping soil salinity changes using remote sensing in Central Iraq. *Geoderma Regional, 2-3,* 21–31.

Yang, L., Huang, C., Liu, G., Liu, J., & Zhu, A. (2015). Mapping soil salinity using a similarity-based prediction approach: a case study in Huanghe River Delta, China. *Chinese Geographical Science,* 1–12.

Zhang, T., Qi, J., Gao, Y., Ouyang, Z., Zeng, S., & Zhao, B. (2015). Detecting soil salinity with MODIS time series VI data. *Ecological Indicators, 52,* 480–489.

Zhang, T., Zeng, S., Gao, Y., Ouyang, Z., Li, B., Fang, C., et al. (2011). Using hyperspectral vegetation indices as a proxy to monitor soil salinity. *Ecological Indicators, 11,* 1552–1562.